AGU PUBLICATIONS

Geophysical Research Letters

RESEARCH LETTER
10.1002/2014GL061570

Key Points:
- Contraction along divergent plate boundaries results from dike emplacement
- Contraction generates extensional structures along divergent plate boundaries
- Surface deformation along divergent plate boundaries may be magma induced

Correspondence to:
D. Trippanera,
daniele.trippanera@uniroma3.it

Citation:
Trippanera, D., V. Acocella, and J. Ruch (2014), Dike-induced contraction along oceanic and continental divergent plate boundaries, *Geophys. Res. Lett.*, *41*, 7098–7104, doi:10.1002/2014GL061570.

Received 17 AUG 2014
Accepted 1 OCT 2014
Accepted article online 2 OCT 2014
Published online 24 OCT 2014

Dike-induced contraction along oceanic and continental divergent plate boundaries

D. Trippanera[1], V. Acocella[1], and J. Ruch[2]

[1]Dipartimento di Scienze, Università Roma Tre, Rome, Italy, [2]Now at KAUST, Thuwal, Saudi Arabia

Abstract The axis of divergent plate boundaries shows extension fractures and normal faults at the surface. Here we present evidence of contraction along the axis of the oceanic ridge of Iceland and the continental Main Ethiopian Rift. Contraction is found at the base of the tilted hanging wall of dilational normal faults, balancing part of their extension. Our experiments suggest that these structures result from dike emplacement. Multiple dike injection induces subsidence above and uplift to the sides of the dikes; the transition in between is accommodated by reverse faults and subsequent peripheral inward dipping normal faults. Our results suggest that contraction is a direct product of magma emplacement along divergent plate boundaries, at various scales, marking a precise evolutionary stage and initiating part of the extensional structures (extension fractures and normal faults).

1. Introduction

Continental and oceanic divergent plate boundaries are the locus of crustal extension. Here along the rift axis, at the surface, common active structures consist of iso-oriented eruptive fissures, extension fractures, and normal faults. Extension fractures are ~10^2 m long and a very few meters wide. Normal faults, often forming grabens or half grabens, are ~10^3 m long; the shallowest part of these faults along the rift axis commonly displays a dilational (tensile) component, of a very few meters, between the footwall and the hanging wall; the latter is often tilted outward [*Gudmundsson*, 1992; *Angelier et al*., 1997; *Acocella*, 2014, and references therein]. Contractional structures have been described, to our knowledge, only in a local case of high-angle reverse faulting due to dike injection reactivating a preexisting normal fault in Iceland [*Gudmundsson et al*., 2008]; despite the importance, this is thus a secondary feature of limited extent.

Here we first provide field evidence of reverse faulting and folding along the oceanic ridge of Iceland and the continental Main Ethiopian Rift (MER). This contraction is found along the rift axis, at the base of the tilted hanging wall of dilational normal faults. We then use experiments to understand the condition of formation of these contractional structures. Our results suggest that these are products of dike injection at the surface along divergent plate boundaries.

Iceland marks the subaerial portion of the Mid-Atlantic Ridge, separating the North American and Eurasian Plates at ~2 cm/yr [e.g., *DeMets et al*., 2010] (Figure 1a). Extension and volcanism focus along the rift axis, in magmatic segments ~10^1 km long and several kilometers wide. These have a dominant volcano and, to their sides along the rift axis, dike-fed eruptive fissures with extension fractures and normal faults, often forming grabens [*Gudmundsson*, 1995; *Wright et al*., 2012]. The MER separates a portion of the Nubia and Somalia plates at 4–6 mm/yr [e.g., *DeMets et al*., 2010]. Similarly to Iceland, in the MER extension and volcanism focus in magmatic segments, each with a dominant felsic volcano, eruptive fissures, extension fractures, and normal faults (Figure 1d) [*Ebinger and Casey*, 2001].

2. Field Analysis

We describe examples of representative contractional structures in Iceland (Krafla and Reykjanes areas; Figures 1b and 1c) and the MER (Fantale area; Figure 1e). Well-exposed contractional structures in Iceland are found on the southern part of the Krafla magmatic segment. For example, here the ~2 km long Grjotagja fault lies on the western boundary of an ~1 km wide graben on an ~2.7 ka lava flow, with cumulative vertical displacement of 5–6 m. The fault has a dilational component, with gaping of a very few meters and hanging wall tilt of 30–35° toward the graben center (Figure 1f). At Grjotagja, the very well-exposed base of the tilted hanging wall consists of a strip parallel to the fault trace, 10^2 m long, of folded and at times chaotic lava

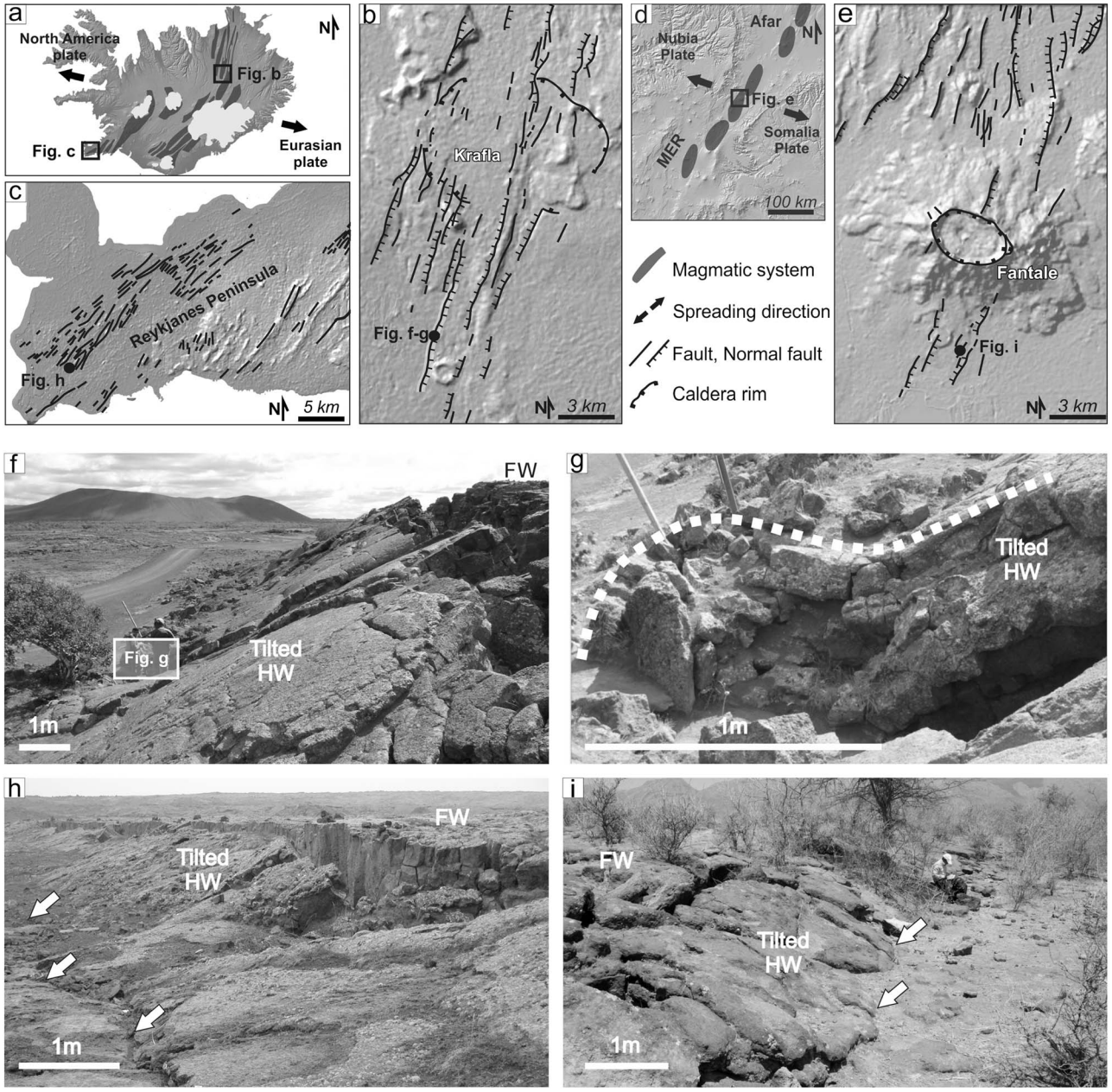

Figure 1. The divergent plate boundaries of (a) Iceland, with insets on the (b) Krafla and (c) Reykjanes areas, and the (d) MER, with inset on (e) Fantale area; the black squares highlight the areas considered in this study. (f) Dilational normal fault with tilted hanging wall (HW) with basal fold at Grjotagja, Krafla (65°37′23.57″N; 16° 53′08.90″W); (g) the details of the fold are shown in Figure 1c. Dilational normal faults with tilted hanging wall with basal reverse faults at (h) Vogar, Reykjanes Peninsula (63°49′23.41″N; 22°36′33.24″W) and (i) Fantale, MER (8°55′35.07″N, 39°54′1.75″E). The arrows highlight the reverse fault trace; FW = footwall.

blocks, indicating localized contraction along the fault. The best exposures systematically reveal a tight cylindrical fold, ~1 m wide and with an ~90° interlimb angle, whose axis is parallel to the fault (Figure 1g). In three balanced cross sections across the normal fault, the associated contraction is 7–20% of the horizontal extension (Figure 2).

Very similar contractional features are found elsewhere along the rift axis of Iceland and of the MER, as in the Vogar (SW Iceland; Figure 1h) and Fantale (central MER; Figure 1i) magmatic segments. Two examples from these areas show narrow (~20 m wide) grabens bordered by normal faults with tilted hanging wall and vertical displacement of a very few meters. The tilted lavas of the hanging wall abruptly terminate above the horizontal lavas of the inner graben, indicating the presence of a thrust or reverse fault, rather than a fold,

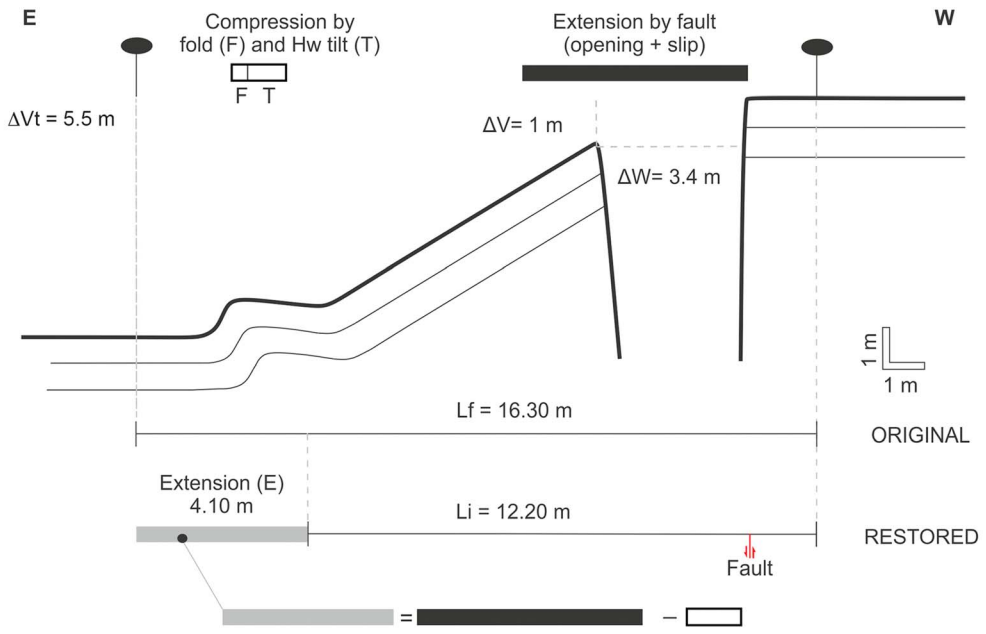

Section	Final lenght (Lf)	Initial lenght (Li)	Total extension	Total compr. fold (F) + tilt (T)	Fold compr. vs tot. ext.	Residual ext. (E)
1	16.30 m	12.20 m	5.40 m	1.30 m	7.4 %	4.10 m
2	25.80 m	22.06 m	5.52 m	1.78 m	10.0 %	3.74 m
3	19.00 m	15.18 m	6.22 m	2.40 m	19.9 %	3.82 m

Figure 2. Example of balanced cross section across the Grjotagja Fault, NE Iceland, reporting the amount of cumulative extension ΔVt (given by the tensile component ΔW plus the vertical displacement down to the base of the tilted hanging wall (HW), assuming a 70° dipping fault) [e.g., *Gudmundsson*, 1992]. The table below reports the amount of extension (also indicated as "ext.") and compression (also indicated as "compr.") along three cross sections of the fault (the above sketch refers to the first case).

parallel to the normal fault. In both cases, the vertical displacement is of very few tens of centimeters, a portion of the vertical displacement (≤1 m) at the contact between the hanging wall and the footwall.

3. Analogue Models

To better understand the mechanism of formation of the contractional features, we use analogue experiments. On the field, the contraction is found on the hanging wall of the active normal faults, whose formation and growth along the axis of divergent plate boundaries may be related to dike emplacement during rifting episodes [e.g., *Rowland et al*., 2007; *Ebinger et al*., 2010]. Here we test whether repeated dike injection may reproduce the observed deformation, that is a normal fault with contraction at the base of the tilted hanging wall. To simulate the repeated dike injection, we insert 0.5 mm thick metal plates into crushed cohesive sand within a $25 \times 45 \times 15$ cm box, with a setup similar to *Mastin and Pollard* [1988] (Figure 3a); 1 cm in the experiments corresponds to ~10^2 m in nature (scaling in *Ruch et al*. [2012]); therefore, the injection of a 0.5 mm thick plate may correspond to one or more rifting episodes [*Ebinger et al*., 2010; *Wright et al*., 2012]. The vertical and horizontal surface deformation are detected through the particle image velocity technique (PIV) and laser scanner (resolution ~5×10^{-2} mm) [*Ruch et al*., 2012].

We have performed 11 experiments. Here we describe a representative model with constant depth (4 cm) to the top of the injected sheets (undeformed map view in Figure 3b); increasing this depth does not vary the deformation pattern. The intrusion of 3 plates forms an elongated depression (~0.2 mm subsidence) above the dike, bordered by two uplifted areas (~0.3 mm of maximum uplift along 8 cm) to the sides. Each transition from the subsided to the uplifted portions initially consists of an inward tilt at the surface; this is subsequently

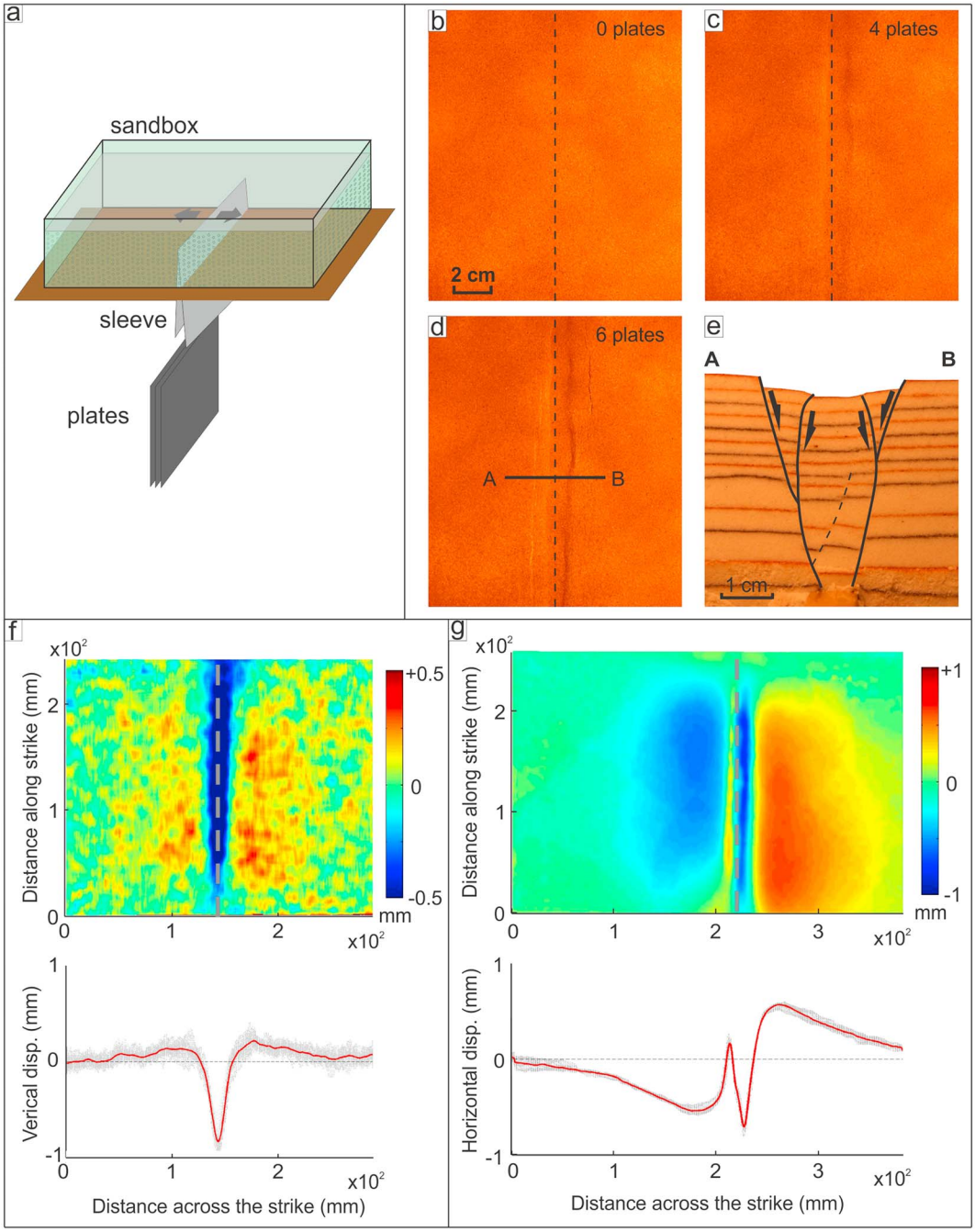

Figure 3. Dike emplacement experiments. (a) Setup: metal plates are injected in the sleeve at the base of the model within the sand; (b) map view of experiment without plate injection; (c) after the injection of 4 plates; (d) after the injection of 6 plates; dashed line indicates position of the slot for injections; (e) section view of the experiment (location of sections in Figure 3d, at a different scale) after the injection of 20 plates; and (f) vertical and (g) horizontal deformation of the surface of the experiment after the injection of 6 plates. In Figure 3f, positive values are uplift, and negative values are subsidence; in Figure 3g, positive values are rightward, and negative values are leftward.

(with 4 injected plates) replaced by a fault, growing in continuity, length, and displacement (Figure 3c). From 6 plates, an outer fault forms and develops on each side of the depression, parallel to and at ~1 cm from the former fault (Figure 3d). The activity of the outer faults significantly reduces that of the inner faults. Between each pair of internal and outer faults, the inward tilt of the surface may reach 20°–30°. Injecting >7–8 plates does not change the deformation pattern. The section view of the final experiment shows that the inner

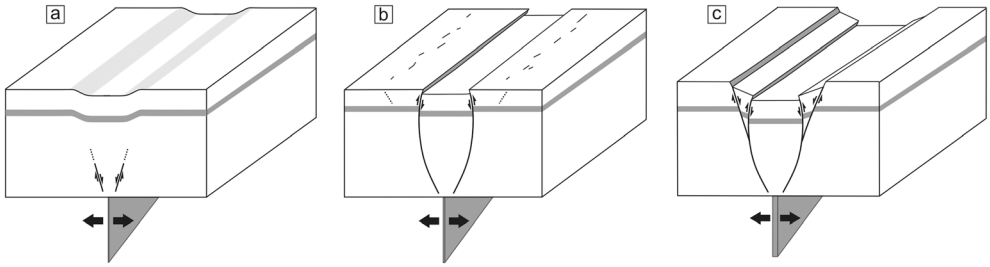

Figure 4. Summary of the main stages of surface deformation due to the emplacement of the dikes. (a) Depression at the surface, (b) inner set of arcuate faults propagating upward and reaching the surface as high-angle reverse faults, and (c) outer set of normal faults propagating downward and merging with the inner faults at depth. The tilted blocks lie between the outer and inner faults.

faults are high angle and arcuate, dipping inward (at the base) and outward (at the top), thus reaching the surface as reverse faults (Figure 3e). The outer faults branch from the area of maximum curvature of the inner faults and are planar and inward dipping, thus normal faults. The direct observation and the displacement variations along the faults in section view show that the inner faults grow upward and the outer faults grow downward. At the surface, uplift and outward horizontal displacement are confined outside the outer faults, progressively approaching zero outward, suggesting negligible border effects along the inner wall of the box; absolute subsidence is confined within the central depression; the areas between each pair of internal and outer fault show inward horizontal motion (Figures 3f and 3g).

4. Discussion and Conclusions

Field data along well-exposed portions of divergent plate boundaries highlight contraction, as tight folds or reverse faults at the base of the tilted hanging wall of dilational normal faults. The possibility to develop a fold or, alternatively, a fault results from the intensity of the relative strain (with regard to the unit volume) at the surface, as suggested by fault propagation fold models; here we will refer for simplicity to the mature stage of development of the contraction, that is reverse faulting.

We simulated dike intrusion to try to explain the contraction at the base of the normal faults. Contraction results from the differential vertical movement induced by the injection of the dike analogues (the plates). This is estimated, at the end of the experiment, at ~1 mm at the surface, or ~10% of the thickness of the injected plates. Injecting the plates induces subsidence above and uplift to their sides; the subsidence is related to the widening of the wedge to be bordered by the arcuate faults above the plates; the uplift results from the lateral compression induced by the plates (Figure 4a) [*Rubin and Pollard*, 1988). The transition from subsidence to uplift is first accommodated by a broad inward tilt of the surface, subsequently replaced by anelastic deformation, when the arcuate high-angle faults propagating upward reach the surface as reverse faults (Figure 4b).

High-angle reverse faults are commonly found with differential vertical movements of adjacent crustal blocks, due to an upward local rotation of the maximum compressive stress, potentially explained by the vault effect above a cavity or, more in general, above a subsiding portion of crust. These structures have been observed in sedimentary basins, basement faulting, calderas, and mining cavities [*Wise*, 1963; *Prucha et al*., 1965; *Given*, 1973; *Vendeville*, 1988; *Roche et al*., 2000; *Merle et al*., 2001; *Acocella*, 2007; *Abe et al*., 2011]. However, a novelty of our study is that the reverse faults may also result from dike emplacement, not necessarily from the activity of any high-angle dip-slip fault, or caldera or mining collapse. While in the latter cases, the maximum compressive stress is subvertical; in our experiment, the maximum compressive stress at the upper plate tip is subhorizontal; approaching the surface, the stress rotates, becoming inward dipping, subvertical, and finally outward dipping, explaining the arcuate geometry of the faults [e.g., *Patton and Fletcher*, 1995; *Bonafede and Danesi*, 1997]. The absolute (above the injection) and relative (with regard to the uplifted portions to the sides of the injections) subsidence induced by the intruded plates causes the inward horizontal displacement of the model above the intrusions. This develops the outer faults (Figure 4c), acting as gravitational structures resulting from the activity of the reverse faults. The outer faults propagate downward, conversely to previous studies on high-angle reverse faults, where the outer faults propagate upward; the nucleation of the outer faults at the surface, where the lithostatic load is least, can be explained by a free surface

effect. Once the normal faults form, they merge with the inward dipping portion of the arcuate faults, forming a continuous structure with localized displacement, locking the reverse faults. Therefore, despite the initial trigger in generating extension at the surface, the reverse faults are transient structures controlling surface deformation under diking. The pattern in the experiment corresponds to a depth/thickness ratio of the top of the dikes $\geq 10^1$. Transferring this to nature, with an inferred mean thickness of a dike complex of ~10^1 m (excluding any host rock in between the dikes), the minimum depth to its top is of ~10^2 m.

Our results suggest that the contraction observed in Iceland and the MER results from dike emplacement, capable to activate dilational normal faults. This process is therefore different from the reactivation of a preexisting normal fault, a local and secondary process generating contraction from extensional structures [e.g., *Gudmundsson et al*., 2008]. The field data and experiments suggest that contraction may develop along grabens with variable width (10^1–10^3 m); however, there is evidence of wider grabens sharing similar features, as being bordered by larger normal faults with inward tilted hanging wall, whose base, often hidden or inaccessible, may undergo larger contraction. These include the ~5 km wide Thingvellir graben (West Volcanic Zone of Iceland), bordered by oppositely verging normal faults with displacement of tens of meters and tilted hanging wall over several tens of meters [*Gudmundsson*, 1987]. Here the base of the hanging wall of the faults, partly covered by sediments or water, hides any contraction, which is nevertheless expected to be relevant. Similarly, the central part of the East Pacific Rise often shows a few kilometers wide and ~100 m deep axial trough, interpreted as a graben due to a narrow and active diking zone [*Chadwick and Embley*, 1998]. The removal of the topographic effect of faulting from the original seafloor bathymetry reveals an inward tilted hanging wall within the trough, possibly resulting from subsurface magmatic deflation [*Carbotte et al*., 2003]. The larger (30–50 km wide) Tendaho Graben, Central Afar, has oppositely verging normal faults with vertical displacement of ~1.6 km and tilted hanging wall ≥10 km wide, also suggesting significant contraction at its base [*Acocella*, 2014, and references therein]. Furthermore, contraction (buckles and anticlines) at the base of tilted hanging walls of normal faults has been described also in magmatic settings outside divergent plate boundaries. These include the Taupo volcanic arc of New Zealand and Kilauea volcano, Hawaii. In the extensional arc of the Taupo Volcanic Zone, contractional structures are observed in trenches; even though these may be tectonically induced [*Seebeck and Nicol*, 2009], there is evidence for magma-assisted rifting along the Taupo Volcanic Zone [*Rowland et al*., 2010]. In Hawaii, the Koa'e fault system, on the western continuation of the east rift zone of Kilauea, shows contractional structures [*Holland et al*., 2006; *Kaven and Martel*, 2007; *Podolsky and Roberts*, 2008] possibly generated by shallow dike emplacement, as suggested by documented intrusions along the Koa'e fault system, as in 1972 [*Swanson et al*., 1976]. These data suggest that contraction within rift zones is not restricted to divergent plate boundaries; rather, it can also be observed in rifts, in general, including extensional volcanic arcs or, at a smaller scale, volcanic rift zones. The common and direct feature for the generation of contractional structures appears to be magma emplacement, in the form of dikes; even though in some cases (Taupo Volcanic Zone), a regional tectonic contribute may not be excluded.

In synthesis, our study suggests that contraction (reverse faults and folds) (1) is found at the surface along the axis of oceanic and continental divergent plate boundaries; (2) may commonly and directly result from magma emplacement, not necessarily from the development or reactivation of preexisting normal faults; and (3) even though probably transient, may generate part of the observed active extensional structures (extension fractures and normal faults) bordering grabens along the axis of divergent plate boundaries, at various scales.

Acknowledgments
Bekele Abebe and Gianluca Norini partly participated to the field analysis. Andrea Giordano helped in the setting up of the experiments. O. Merle and an anonymous reviewer provided the helpful suggestions. Financed with PRIN 2009 funds (2009H37M59, responsible V. Acocella). Any user can access the data of this work by contacting the corresponding author.

The Editor thanks Olivier Merle and an anonymous reviewer for their assistance in evaluating this paper.

References

Abe, S., H. van Gent, and J. L. Urai (2011), DEM simulation of normal faults in cohesive materials, *Tectonophysics*, *512*, 12–21, doi:10.1016/j.tecto.2011.09.008.

Acocella, V. (2007), Understanding caldera structure and development: An overview of analogue models compared to natural calderas, *Earth Sci. Rev.*, *85*, 125–160, doi:10.1016/j.earscirev.2007.08.004.

Acocella, V. (2014), Structural control on magmatism along divergent and convergent plate boundaries: Overview, model, problems, *Earth Sci. Rev.*, *136*, 226–288, doi:10.1016/j.earscirev.2014.05.006.

Angelier, J., F. Bergerat, O. Dauteuil, and T. Villemin (1997), Effective tension-shear relationships in extensional fissure swarms, axial rift zone of northeastern Iceland, *J. Struct. Geol.*, *19*, 673–685, doi:10.1016/S0191-8141(96)00106-X.

Bonafede, M., and S. Danesi (1997), Near-field modifications of stress induced by dyke injection at shallow depth, *Geophys. J. Int.*, *130*, 435–448, doi:10.1111/j.1365-246X.1997.tb05659.x.

Carbotte, S. M., W. B. F. Ryan, W. Jin, M. Cormier, E. Bergmanis, J. Sinton, and S. White (2003), Magmatic subsidence of the East Pacific Rise (EPR) at 18°14′S revealed through fault restoration of ridge crest bathymetry, *Geochem., Geophys., Geosyst.*, *4*(1), 1008, doi: 10.1029/2002GC000337.

Chadwick, W., and R. W. Embley (1998), Graben formation associated with recent dike intrusions and volcanic eruptions on the mid-ocean ridge, *J. Geophys. Res.*, *103*, 9807–9825, doi:10.1029/97JB02485.

DeMets, C., R. G. Gordon, and D. F. Argus (2010), Geologically current plate motions, *Int. J. Geophys.*, *181*, 1–80.

Ebinger, C., A. Ayele, D. Keir, J. Rowland, G. Yirgu, T. Wright, M. Belachew, and I. Hamling (2010), Length and timescales of rift faulting and magma intrusion: The Afar rifting cycle from 2005 to present, *Annu. Rev. Earth Planet. Sci.*, *38*, 439–466, doi:10.1146/annurev-earth-040809-152333.

Ebinger, C. J., and M. Casey (2001), Continental breakup in magmatic provinces: An Ethiopian example, *Geology*, *29*, 527–530, doi:10.1130/0091-7613(2001)029<0527.

Given, I. A. (Ed.) (1973), *Mining Engineering Handbook*, Part City Press, New York.

Gudmundsson, A. (1987), Tectonics of the Thingvellir fissure swarm SW Iceland, *J. Struct. Geol.*, *9*, 61–69.

Gudmundsson, A. (1992), Formation and growth of normal faults at the divergent plate boundary in Iceland, *Terranova*, *4*, 464–471.

Gudmundsson, A. (1995), Infrastructure and mechanics of volcanic systems in Iceland, *J. Volcanol. Geotherm. Res.*, *64*, 1–22.

Gudmundsson, A., N. Friese, I. Galindo, and S. L. Philipp (2008), Dike-induced reverse faulting in a graben, *Geology*, *36*, 123, doi:10.1130/G24185A.1.

Holland, M., J. L. Urai, and S. Martel (2006), The internal structure of fault zones in basaltic sequences, *Earth Planet. Sci. Lett.*, *248*, 301–315, doi:10.1016/j.epsl.2006.05.035.

Kaven, J. O., and S. J. Martel (2007), Growth of surface-breaching normal faults as a three-dimensional fracturing process, *J. Struct. Geol.*, *29*, 1463–1476, doi:10.1016/j.jsg.2007.05.007.

Mastin, L. G., and D. D. Pollard (1988), Surface deformation and shallow dike intrusion processes at Inyo Craters, Long Valley, Calif., *J. Geophys. Res.*, *93*, 13,221–13,235, doi:10.1029/JB093iB11p13221.

Merle, O., N. Vidal, and B. van Wyk de Vries (2001), Experiments on vertical basement fault reactivations below volcanoes, *J. Geophys. Res.*, *106*, 2153–2162, doi:10.1029/2000JB900352.

Patton, T. L., and R. C. Fletcher (1995), Mathematical block-motion model for deformation of a layer above a buried fault of arbitrary dip and sense of slip, *J. Struct. Geol.*, *17*, 1455–1472, doi:10.1016/0191-8141(95)00034-B.

Podolsky, D. M. W., and G. P. Roberts (2008), Growth of the volcano-flank Koa'e fault system, Hawaii, *J. Struct. Geol.*, *30*, 1254–1263, doi:10.1016/j.jsg.2008.06.006.

Prucha, J. J., J. A. Graham, and R. P. Nickelsen (1965), Basement-controlled deformation in Wyoming province of Rocky Mountains foreland, *Am. Assoc. Petrol. Géol. Bull.*, *49*, 966–992.

Roche, O., T. H. Druitt, and O. Merle (2000), Experimental study of caldera formation, *J. Geophys. Res.*, *105*, 395–416, doi:10.1029/1999JB900298.

Rowland, J. V., E. Baker, C. J. Ebinger, D. Keir, T. Kidane, J. Biggs, N. Hayward, and T. J. Wright (2007), Fault growth at a nascent slow-spreading ridge: 2005 Dabbahu rifting episode, Afar, *Geophys. J. Int.*, *171*, 1226–1246, doi:10.1111/j.1365-246X.2007.03584.x.

Rowland, J. V., C. J. N. Wilson, and D. M. Gravley (2010), Spatial and temporal variations in magma-assisted rifting, Taupo Volcanic Zone, New Zealand, *J. Volcanol. Geotherm. Res.*, *190*, 89–108.

Rubin, M., and D. D. Pollard (1988), Dike-induced faulting in rift zones of Iceland and Afar, *Geology*, *16*, 413–417.

Ruch, J., V. Acocella, N. Geshi, A. Nobile, and F. Corbi (2012), Kinematic analysis of vertical collapse on volcanoes using experimental models time series, *J. Geophys. Res.*, *117*, B07301, doi: 10.1029/2012JB009229.

Seebeck, H., and A. Nicol (2009), Dike intrusion and displacement accumulation at the intersection of the Okataina Volcanic Centre and Paeroa Fault zone, Taupo Rift, New Zealand, *Tectonophysics*, *475*, 575–585, doi:10.1016/j.tecto.2009.07.009.

Swanson, B. D. A., W. A. Duffield, and R. Fiske (1976), Displacement of the South Flank of Kilauea Volcano: The result of forceful intrusion of magma into the rift zones, *Geol. Surv. Prof. Pap.*, *963*, 1–39.

Vendeville, B. (1988), Modèles expérimentaux de fracturation de la couverture contrôlée par des failles normales dans le socle, *C. R. Acad. Sci. Paris, Sér. II*, *307*, 1013–1019.

Wise, D. U. (1963), Keystone faulting and gravity sliding driven by basement uplift of Owl Creek Mountains, Wyoming, *Am. Assoc. Pet. Geol. Bull.*, *47*, 586–596.

Wright, T. J., et al. (2012), Geophysical constraints on the dynamics of spreading centres from rifting episodes on land, *Nature*, *5*, 242–250, doi:10.1038/ngeo1428.